

Electrocatalysis

Synergistic C–N Coupling for Efficient Cyclohexanone Oxime Synthesis from Ambient Air by Supported Molecular Catalysts

Chen Zhang⁺, Shu-Lin Meng⁺, Yan-Nan Jing, Cheng Wang, Xin-Ling Zhang, Hai-Xu Wang, Chen-Ho Tung, and Li-Zhu Wu*

Abstract: Electrocatalytic synthesis of cyclohexanone oxime from rich nitrogen resources is a promising alternative to traditional industrial processes. However, the difficulties in unraveling atomic-scale catalytic mechanisms and managing selective C–N coupling still pose great challenges to realizing considerable yield and selectivity, and therefore rational catalyst design to boost collaborative C–N coupling for oxime synthesis is particularly attractive. In the present work, molecular catalysts are demonstrated to be unique for oxime synthesis under mild conditions, i.e., iron bis(pyridyl)amine-bipyridine (FeBPAbipyH) modified MWCNTs@CP (multi-walled carbon nanotubes coated carbon fiber paper) cathodes produced cyclohexanone oxime from NO₂[−] and cyclohexanone, attaining mass-specific efficiency of 87.00 mg h^{−1} cm^{−2} mg_{cat}^{−1}, Faradaic efficiency (FE) of 77.3%, and exclusive carbon selectivity, which is the best efficiency known to date in H-cell. Mechanistic studies showed that the FeBPAbipyH molecular skeleton exhibited intimate interaction with both cyclohexanone and NO₂[−], and catalyzed selective NO₂[−]-to-NH₂OH reduction for C–N bond in situ. The in-depth understanding of substrate-catalyst interactions and synergic C–N coupling from molecular points of view offers valuable insights to boost collaborative synthesis of organic nitrogen compounds. Further integrating plasma-driven N₂ oxidation and electrocatalysis enabled cyclohexanone oxime formation at 61.73 mg h^{−1} cm^{−2} mg_{cat}^{−1} on the FeBPAbipyH/MWCNTs@CP electrode, and the whole synthetic and separation process is projected to be profitable with a promising cost of \$2709 ton^{−1}, which is much lower than the breakeven point (~\$10 000 ton^{−1}), representing a sustainable pathway to nitrogenous chemical synthesis from abundant resources under ambient conditions.

Introduction


Cyclohexanone oxime, as the key precursor for nylon-6, has an ever-growing annual demand of nearly 10 million tons.^[1] The conventional route to industrial cyclohexanone oxime synthesis relies on the stoichiometric condensation between cyclohexanone (CYC) and hydroxylamine sulfate, which is obtained by either NO reduction with H₂ or ammonia oxidation with H₂O₂.^[2] In these reaction processes, the requirement of precious metal catalysts and a large amount of toxic and corrosive agents results in poor step economy, atomic economy, and redox economy.^[3] By leveraging the

C–N coupling of carbon-containing organic compounds with *NH₂OH generated in situ during electrocatalytic reduction of nitrogenous resource molecules (NO, NO₂[−]), the use of stoichiometric NH₂OH, and thus excessive oxidants and acids, can be avoided.^[4–6] In this context, it is necessary to forge controllable N–O bond dissociation of NO_x[−] substrate and moderate N–H bond formation to deliver *NH₂OH, along with C–N coupling between reactive *NH₂OH and cyclohexanone, overcoming various side reactions such as excessive N–H bond formation to deliver NH₃, solo C–H bond formation to yield cyclohexanol, and H–H bond formation to cause H₂ evolution reaction. Recently, a growing library of catalysts has been documented for cyclohexanone oxime electrosynthesis, including metals,^[7] alloys,^[8,9] metal oxides,^[10] sulfides,^[11] and nonmetals.^[12] The pioneering research on these catalysts has greatly advanced cyclohexanone oxime yield rate and Faradaic efficiency (FE), and the highest mass-specific yield rate in H-cell reached 32.59 mg h^{−1} cm^{−2} mg_{cat}^{−1} (FE = 47.6% at −0.90 V vs. Ag/AgCl)^[8] using PdCuAg-BiInene high-entropy alloy, while Rutile TiO₂ delivered the best FE of 68.2% so far (yield rate = 14.4 mg h^{−1} cm^{−2} at 30 mA cm^{−2}).^[10] For selective cyclohexanone oxime synthesis, the efficiency is particularly determined by the spatiotemporal collaboration of active sites, which should present strong and balanced interaction with cyclohexanone and nitrogenous substrates, modest hydrogenation ability to accumulate *CYC and *NH₂OH intermediates, and close contact to enable timely C–N coupling. Therefore, atomic-scale

[*] C. Zhang⁺, S.-L. Meng⁺, Y.-N. Jing, C. Wang, X.-L. Zhang, H.-X. Wang, C.-H. Tung, L.-Z. Wu
 Key Laboratory of Photochemical Conversion and Optoelectronic Materials, New Cornerstone Science Laboratory, Technical Institute of Physics and Chemistry, Chinese Academy of Sciences, Beijing 100190, China
 E-mail: lzwu@mail.ipc.ac.cn

C. Zhang⁺, S.-L. Meng⁺, Y.-N. Jing, C. Wang, X.-L. Zhang, H.-X. Wang, C.-H. Tung, L.-Z. Wu
 School of Future Technology, University of Chinese Academy of Sciences, Beijing 100049, China

[+] Both authors equally contributed to this work

 Additional supporting information can be found online in the Supporting Information section

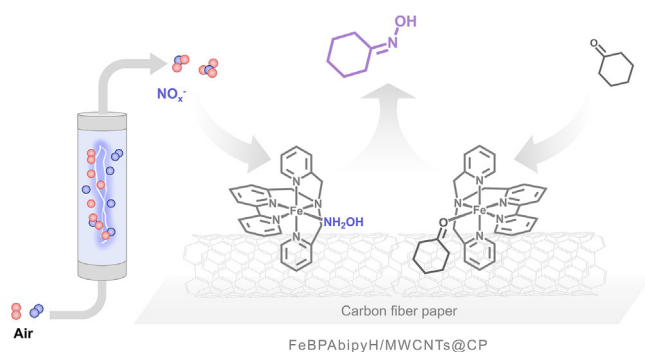


Figure 1. Cyclohexanone oxime synthesis by collaborative C–N coupling with molecular FeBPAbipyH catalyst immobilized on MWCNTs.

understandings of the interplay of catalytic sites with substrates and intermediates are highly desirable.

Molecular catalysts have definite structures and coordination environments, which are expected to achieve controllable NO_2^- reduction to $^*\text{NH}_2\text{OH}$ by adjusting electron and proton transfer kinetics via structural design and to offer convenient access to unravel the landscape of electrocatalytic multistep reactions. Simultaneously, molecular catalysts exhibit high atom utilization and can be immobilized on functional electrodes to boost rapid electron transfer, thus realizing extremely high intrinsic activities, which have been testified to in multielectron and multiproton transformations.^[13–16] However, the use of molecular catalysts to realize synergic C–N coupling for selective cyclohexanone oxime synthesis is rather elusive.

With these in mind, we attempted to examine the iron bis(pyridyl)amine-bipyridine (FeBPAbipyH) catalyst skeleton with a well-defined active site for cyclohexanone oxime synthesis. To our delight, the FeBPAbipyH skeleton anchored onto conductive multi-walled carbon nanotubes (MWCNTs@CP) here enabled selective electrocatalytic cyclohexanone oxime synthesis from NO_2^- . The experimental results showed that cyclohexanone oxime was synthesized with 77.3% FE on FeBPAbipyH/MWCNTs@CP cathode at -0.40 V vs. RHE, with 100% ketone-to-oxime selectivity and a mass-specific yield rate of $87.00 \text{ mg h}^{-1} \text{ cm}^{-2} \text{ mg}_{\text{cat}}^{-1}$. Mechanistic studies revealed that the FeBPAbipyH skeleton exhibited a strong interaction with $^*\text{NH}_2\text{OH}$ and a commensurate binding with cyclohexanone and NO_2^- , which favored NO_2^- reduction to NH_2OH over NH_3 , thus facilitating advantageous C–N coupling. The highest mass-specific cyclohexanone oxime yields and FEs have been achieved among reported works in H-cell (Table S1). Even after 12 h of continuous electrolysis, the catalyst maintained good stability. Further, using NO_x^- generated directly from plasma oxidation of air had the cyclohexanone oxime yield of $61.73 \text{ mg h}^{-1} \text{ cm}^{-2} \text{ mg}_{\text{cat}}^{-1}$ on the FeBPAbipyH/MWCNTs@CP electrode (Figure 1). This work expounds the key factors to improve the efficiency of electrocatalytic C–N coupling from the perspective of molecular design, which enlightens the catalyst development for efficient and economic synthesis of nitrogenous compounds from ambient air.

Results and Discussion

Electrocatalytic Cyclohexanone Oxime Synthesis

The FeBPAbipyH complex was used as the model catalyst and immobilized on MWCNTs supported by porous carbon paper (CP) as the working electrode. By cyclic voltammetry (CV) (Figure S5), the loading of electrochemically active catalyst (FeBPAbipyH) on the electrode surface was calculated to be $0.3 \mu\text{g cm}^{-2}$.^[17,18] X-ray photoelectron spectroscopy (XPS) showed that the Fe element could be detected on the FeBPAbipyH/MWCNTs@CP electrode, but it was not found on the MWCNTs@CP electrode (Figures S6 and S7). The change of the binding energy of Fe^{2+} before and after loading FeBPAbipyH on MWCNTs@CP electrode confirmed the interaction between FeBPAbipyH and MWCNTs (Figure S8). In addition, scanning electron microscope and energy-dispersive X-ray (EDX) mapping confirmed the uniform distribution of the catalyst on CNTs (Figure S9).

The proof-of-concept electrosynthesis of cyclohexanone oxime was verified in the aqueous solution of 500 mM phosphate buffer (pH = 5.30), 100 mM NaNO_2 and 10 mM cyclohexanone within an H-type cell. During the reaction, the only gaseous product, H_2 was quantified by gas chromatography (FE < 0.5%), the only inorganic product, NH_3 was quantified by ^1H NMR (Figures S10 and S11), and the only organic product, cyclohexanone oxime, was quantified by ^1H NMR and gas chromatography-mass spectrometry (GC-MS) (Figures S12–S15). All the ^1H NMR peaks of the electrolyte after the reaction were completely matched with those of the cyclohexanone and cyclohexanone oxime standards. To confirm the source of cyclohexanone oxime, we used cyclohexanone as the C-source and $^{15}\text{NO}_2^-$, $\text{NH}_3\cdot\text{H}_2\text{O}$, $\text{N}_2\text{H}_4\cdot\text{H}_2\text{O}$, and $\text{NH}_2\text{OH}\cdot\text{HCl}$ as the N-source instead of $\text{Na}^{14}\text{NO}_2$ (Figure 2a). When $^{15}\text{NO}_2^-$ was used, ^{15}N -labeled cyclohexanone oxime was obtained, judging from the GC-MS signal at 114.1. Cyclohexanone oxime was also formed using NO as a nitrogen source (Figure S16), but could not be detected using NO_3^- instead of NO_2^- (Figure S17). When $\text{NH}_3\cdot\text{H}_2\text{O}$ and $\text{N}_2\text{H}_4\cdot\text{H}_2\text{O}$ were used as N-source, cyclohexanone oxime was not detected. When $\text{NH}_2\text{OH}\cdot\text{HCl}$ was used as N-source, cyclohexanone oxime could be generated immediately at room temperature even under an open circuit, which showed that the condensation of NH_2OH and cyclohexanone was a spontaneous process. At the same time, cyclohexanone oxime was not detected at the open circuit potential (OCP) or in the absence of cyclohexanone or NaNO_2 . All of the results show that the production of cyclohexanone oxime is an electrochemical process, necessitating NaNO_2 and cyclohexanone as N-source and C-source, respectively, and NH_2OH and NO are key intermediates in the reaction process.

Next, catalysts with different metal centers were evaluated by coordinating the ligand skeleton with Fe^{2+} , Co^{2+} , Ni^{2+} , and Mn^{2+} and loading different complexes onto the MWCNT@CP electrode following the same procedures (M-BPAbipyH/MWCNT@CP, M = Fe, Co, Ni, and Mn). Under parallel electrocatalytic tests (Figure 2b), NH_3 in combination with cyclohexanone oxime constituted nearly 100% FE, while

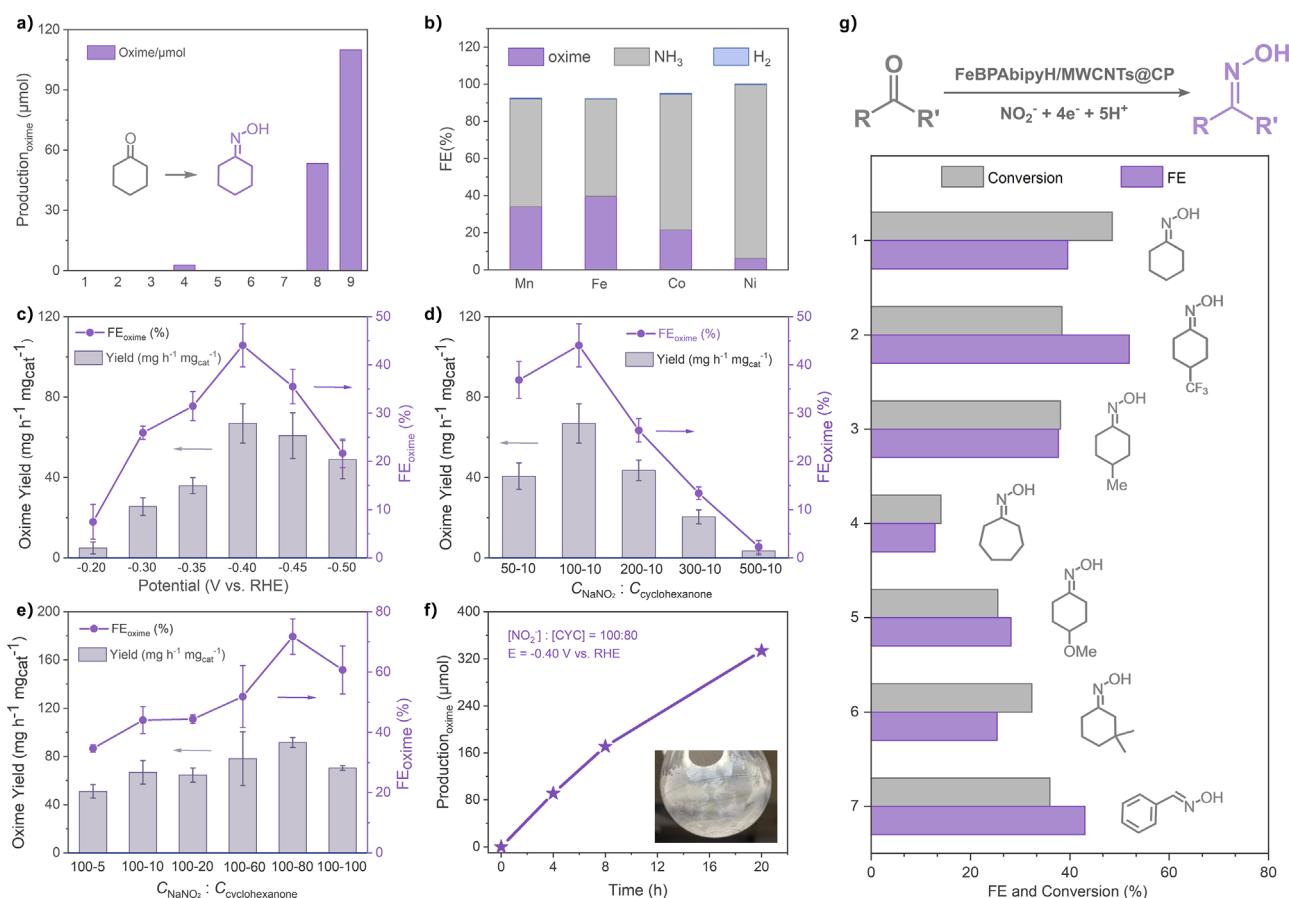


Figure 2. a) Control experiments of cyclohexanone oxime electrocatalysis. 1-no electricity; 2-no N-source; 3-no C-source; 4-MWCNTs@CP without Fe complex; 5-CP electrode without MWCNT or Fe complex; 6-NH₃·H₂O as N-source; 7-N₂H₄·H₂O as N-source; 8-standard; 9-NH₂OH·HCl as N-source (no electricity). b) The product distribution using metal bis(pyridyl)amine-bipyridine complex-modified MWCNTs@CP electrodes with different metal centers (Mn²⁺, Fe²⁺, Co²⁺, Ni²⁺). c)–e) Effects of applied potential and substrate concentration (mmol L⁻¹) ratio on cyclohexanone oxime yield and FE. f) The change of cyclohexanone oxime yield with time during continuous electrolysis for 20 h. Inset: the isolated cyclohexanone oxime after electrolysis. g) The yield and FE of oximes using different ketone or aldehyde substrates (0.01 M) and NO₂⁻ (0.1 M) under the same conditions.

direct cyclohexanone reduction (C–H bond formation) and H₂ evolution (H–H bond formation) were not observable, which excluded the formation of other byproducts. The FE of M-BPAbipyH/MWCNT@CP electrodes for cyclohexanone oxime displayed Fe²⁺ > Mn²⁺ > Co²⁺ > Ni²⁺, where the FeBPAbipyH/MWCNT@CP electrode attained the best FE of 39.58%. The residual part of FE went dominantly to NH₃. The results show that M-BPAbipyH/MWCNT@CP electrodes with earlier transition metal centers (Fe²⁺ and Mn²⁺) favor C–N coupling, while late transition metal centers (Co²⁺ and Ni²⁺), due to the strong N–H bond formation tendency, induce NO₂⁻ over-reduction to NH₃, thus missing C–N coupling.

Given that the electrocatalytic synthesis of cyclohexanone oxime requires an orchestration of electron transfer, proton transfer, mass transfer, and C–N bond formation, the electrochemical performance of cyclohexanone oxime synthesis on the FeBPAbipyH/MWCNTs@CP was tested in the potential range of –0.20 to –0.50 V vs. RHE. The conversion and FE showed a volcanic dependence on catalyst loading, which attained optimum at an FeBPAbipyH loading

of 46.7 μg cm⁻² (Figure S18). As shown in Figure 2c, the FE for cyclohexanone oxime synthesis followed a volcano-shaped trend. At –0.40 V vs. RHE, the production rate peaked at 64.72 mg h⁻¹ cm⁻² mg_{cat}⁻¹. Under –0.20 V vs. RHE, the driving force of electrocatalytic NO₂RR was small, and less NH₂OH was generated, resulting in lower FE of NH₃ and cyclohexanone oxime. More negative potentials enhanced NH₂OH production, which led to the increased FE of NH₃ and cyclohexanone oxime. However, when the potential was too negative, the generated hydroxylamine was quickly reduced to NH₃ before it could combine with cyclohexanone, resulting in a greater tendency of NH₃ synthesis and the decline of cyclohexanone oxime FE. Furthermore, the molar concentrations of cyclohexanone and NO₂⁻ were studied (Figure 2d,e). Excessive concentrations of NO₂⁻ (>100 mM) exasperated the mismatch of cyclohexanone and NO₂⁻ concentrations, thus inhibiting cyclohexanone oxime production (Figure 2d). Increasing the concentrations of cyclohexanone gradually promoted the formation of cyclohexanone oxime. However, excessive cyclohexanone led to not only the decline of NH₂OH production, but also phase separation in the

cathode electrolyte, which hinder the encounter of cyclohexanone and NH_2OH . Under optimal conditions (100 mM NO_2^- and 80 mM cyclohexanone at -0.40 V vs. RHE), the yield of cyclohexanone oxime was $87.00 \text{ mg h}^{-1} \text{ cm}^{-2} \text{ mg}_{\text{cat}}^{-1}$ and the FE reached 77.3%, which reached the highest yield and FE among reported works in literature with an H-cell, highlighting the advantageous activity and selectivity of molecular catalysts.

In addition to activity and selectivity, the stability and durability of the FeBPAbipyH/MWCNTs@CP electrode were also evaluated (Figures 2f, S19, and S20). In the process of continuous electrolysis for 20 h, the yield of cyclohexanone oxime remained unchanged in the first 8 h and then decreased slightly in the following 12 h due to the significant consumption of NO_2^- (from 100 to 48 mM), and cyclohexanone concentrations (from 80 to 50 mM) as well as buffer capacity (Figure 2f). This was also reflected by the change of current density over long-term electrolysis. The current density of the system remained stable for the first 12 h and then gradually declined with the decrease of substrate concentration. Any variation of the ultraviolet–visible (UV–vis) absorption spectrum, SEM, and EDX before and after electrolysis of the FeBPAbipyH/MWCNTs@CP electrode was unnoticeable (Figures S21 and S22), further confirming the excellent stability of the FeBPAbipyH/MWCNTs@CP electrode in the electrosynthesis of cyclohexanone oxime.

The system presented broad applicability to aldehyde and ketone substrates besides cyclohexanone (Figures 2g and S23–S28). In the presence of methyl (3), electron-donating $-\text{OMe}$ (5) or electron-withdrawing $-\text{CF}_3$ (2) groups, the corresponding oxime synthesis proceeded smoothly, maintaining $\sim 40\%$ FE. Using cycloheptanone (4) and 3,3-dimethyl cyclohexanone (6), oxime synthesis was also observed with lower conversion and selectivity due to the greater steric hindrance and reduced solubility in the aqueous electrolyte, which disfavor the interaction of substrates with catalyst and C–N coupling with NH_2OH . Moreover, benzyl oxime synthesis with 36% conversion and 43% FE fully demonstrated the applicability of the FeBPAbipyH molecular catalyst platform in the production of various oxime compounds.

Mechanistic Studies

To guarantee selective C–N coupling between NH_2OH and cyclohexanone, the catalyst should interact with both cyclohexanone and nitrogenous substrates. First, the interaction of FeBPAbipyH with cyclohexanone, NO_2^- , NH_2OH , $\text{NH}_3\cdot\text{H}_2\text{O}$, and cyclohexanone oxime was proved by UV–vis absorption, in which FeBPAbipyH had three absorption peaks at 530, 400, and 345 nm. The addition of NaNO_2 , NH_2OH , and cyclohexanone oxime significantly enhanced the absorbances of the solution due to the stronger ligand field induced by the lone pair of N atom as a good σ -donor^[19] (Figure 3a). The UV–vis absorbances were quite different from the mathematical sum-up of FeBPAbipyH plus NaNO_2 , NH_2OH , or cyclohexanone oxime (Figure S29), indicating that FeBPAbipyH interacted strongly with NO_2^- and NH_2OH . The coordination between cyclohexanone and

catalyst was also corroborated by ^1H NMR, where the signals of bipyridine and $-\text{CH}_2-$ units nearby the amine-N ligand shifted to lower fields (Figure S30). The intimate binding of FeBPAbipyH with NO_2^- favored selective multielectron NO_2^- reduction, and the interaction with NH_2OH stabilized in situ generated hydroxylamine intermediate, which was easily captured by adjacent cyclohexanone to accomplish C–N coupling. According to the absorbance variation at different substrate concentrations (Figure S31–S35), the complexation constants of different components with FeBPAbipyH were calculated. The coordination constants of the catalyst with NO_2^- , cyclohexanone, and cyclohexanone oxime were similar, ranging from 65 to 85 M^{-1} , and the coordination constant of the catalyst with $\text{NH}_3\cdot\text{H}_2\text{O}$ was 17 M^{-1} , while the coordination constant of the catalyst with NH_2OH was as high as 3049 M^{-1} . The similar coordination constants of cyclohexanone and NO_2^- represented their similar binding abilities to FeBPAbipyH, thus ensuring the balanced adsorption and reactivity of carbonaceous and nitrogenous substrates, which maximized the chances for C–N coupling and minimized sole cyclohexanone reduction (C–H bond formation) or excessive NO_x^- reduction (N–H bond formation) side reactions, in turn contributing to the excellent selectivity to cyclohexanone oxime. Therefore, when the concentration ratio of NaNO_2 to cyclohexanone was close to 1:1, the best FE of cyclohexanone oxime could be obtained, which was consistent with the electrolytic experimental results in Figure 2d,e.

When the FeBPAbipyH catalyst was supported on the MWCNTs@CP electrode, the interaction with NO_2^- and cyclohexanone was further evidenced by OCP measurement, which reflected the change of the inner Helmholtz layer.^[20–23] When 0.1 M NO_2^- and 0.01 M cyclohexanone were injected, the OCP of the FeBPAbipyH/MWCNTs@CP electrode changed more obviously (222 mV) than that of the MWCNTs@CP (192 mV) and CP electrode (155 mV) (Figure 3b), indicating that more substrates were adsorbed in the inner Helmholtz layer. In the presence of 0.01 M cyclohexanone, the greatest shift of the OCP was also observed for the FeBPAbipyH/MWCNTs@CP electrode (Figure S36). These results showed that the incorporation of FeBPAbipyH active sites enhanced the adsorption of substrate on the electrode, which favored selective NO_2^- reduction and adjacent C–N coupling reaction.

The ideal catalyst for cyclohexanone oxime electrosynthesis requires not only strong and balanced interaction with both C- and N-substrates, but also weak hydrogenation capacity of accumulated $^*\text{CYC}$ and $^*\text{NH}_2\text{OH}$ intermediates and oxime product. To evaluate the hydrogenation ability of the FeBPAbipyH/MWCNTs@CP electrode, the linear sweep voltammetry (LSV) curve of the electrode was measured in 0.5 M PBS with and without substrate. As shown in Figure 3c, after adding cyclohexanone into PBS buffer, a retarded onset potential and a lower current density confirmed that the electrode interacted with cyclohexanone but was incapable of cyclohexanone hydrogenation, thus preventing the sole cyclohexanone reduction side reaction to cyclohexanol. Indeed, in the potentiostatic electrolysis experiment, cyclohexanone reduction could not observably proceed (Figure S37). On the contrary, with the addition of NaNO_2 or NO (Figure S38),

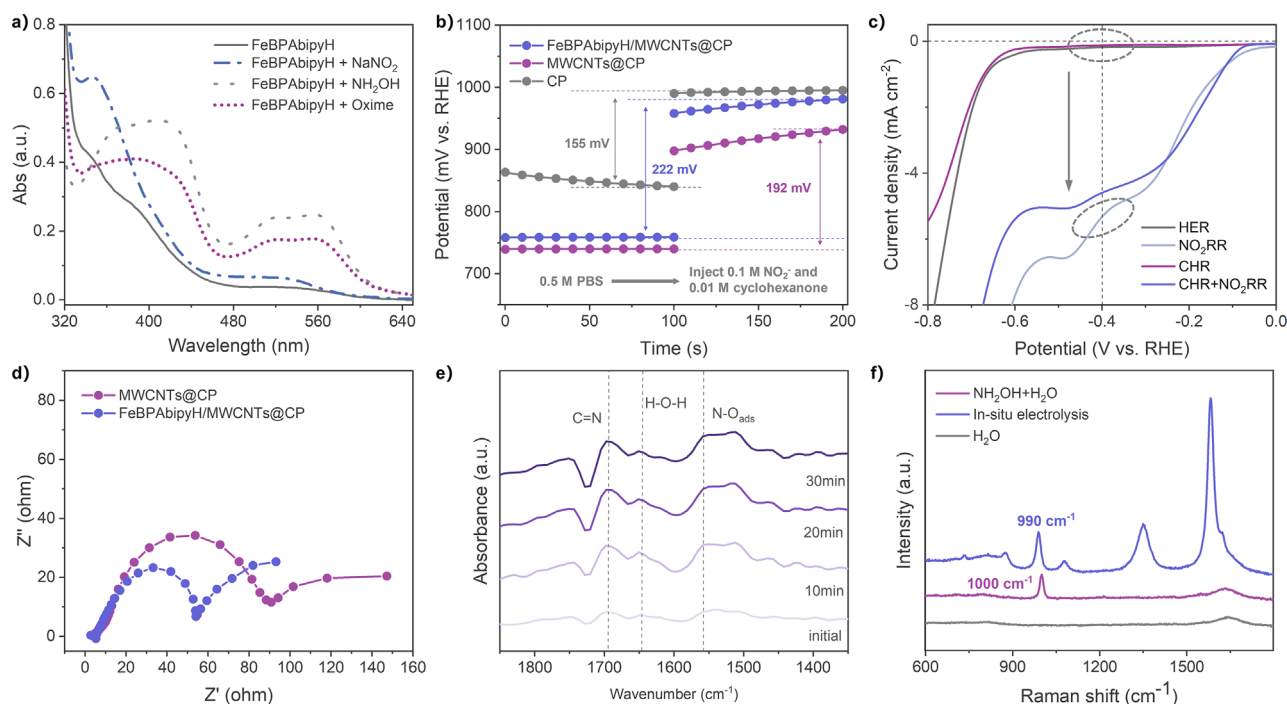


Figure 3. a) UV-vis absorption spectra of the FeBPAbipyH complex with different substrates. b) OCP curve of CP, Fe-complex free MWCNTs@CP and FeBPAbipyH/MWCNTs@CP electrodes with and without substrate. c) LSV of HER (0.5 M PBS), NO₂RR (0.5 M PBS+0.08 M cyclohexanone), NO₂RR (0.5 M PBS+0.1 M NO₂⁻), and CHR + NO₂RR (0.5 M PBS+0.1 M NO₂⁻+0.08 M cyclohexanone) on FeBPAbipyH/MWCNTs@CP electrodes. d) EIS of FeBPAbipyH/MWCNTs@CP and MWCNTs@CP in 0.5 M PBS, 0.1 M NO₂⁻ and 0.01 M cyclohexanone. e) In situ IR spectroscopy. f) In situ Raman spectroscopy.

the current density increased significantly, indicating that the reduction of NO₂⁻ and NO was more active than HER. In the process of NO₂RR, the current density decreased slightly after adding cyclohexanone to the electrolyte, indicating that the added cyclohexanone and NO₂⁻ competed with each other to bind catalytic sites,^[24,25] which was beneficial to the coupling of *CYC and *NH₂OH intermediates. Once cyclohexanone oxime formed, LSV and electrolysis experiments showed no further reduction occurred (Figure S39). In the selected potential range, proton, cyclohexanone, and cyclohexanone oxime reduction hardly started. Especially under the optimum potential, the $j_{\text{NO}_2\text{RR}}$ was 42.5 times that of j_{CHR} (Figure 3c), so that the ketone-to-oxime selectivity could attain almost 100%.

On the basis of balanced substrate binding and selective NO₂⁻ reduction, rapid and continuous electron transfer is important for effective multielectron cyclohexanone oxime synthesis, which was verified by electrochemical impedance spectroscopy (EIS). The charge transfer resistance was directly reflected by the radius of the semicircle.^[26] As shown in Figure S40, the charge transfer resistance of the FeBPAbipyH/MWCNTs@CP and MWCNTs@CP was much smaller than that of CP, indicating that loading FeBPAbipyH and MWCNTs on CP greatly improved the kinetics of cyclohexanone oxime electrosynthesis. Compared with MWCNTs@CP, the charge transfer resistance of the FeBPAbipyH/MWCNTs@CP was smaller (Figure 3d), evidencing the catalytic role of FeBPAbipyH to reduce the barriers for multielectron cyclohexanone oxime synthesis.

This was consistent with the greater current density of the FeBPAbipyH/MWCNTs@CP in the potentiostatic electrolysis experiment (Figure S41).

To deeply understand the reaction mechanism, the reaction process of cyclohexanone oxime synthesis was tracked by in situ spectroscopy and DFT calculation. In situ IR spectroscopy (Figure 3e) showed a distinct and accumulating peak at 1694 cm⁻¹ over time, marking the formation of the C=N bond in the cyclohexanone oxime product.^[27] Raman spectrum (Figures 3f and S42) shows that free hydroxylamine (⁺NH₂OH) presented a $\nu(\text{N}-\text{O})$ mode at 1000 cm⁻¹,^[28] while in the in situ electrolysis process, the signal appeared at 990 cm⁻¹, which shifted to lower wavenumbers by 10 cm⁻¹ from free hydroxylamine. Although *NH₂OH intermediate could be detected spectroscopically in situ during NO₂⁻ reduction (Figure S43), quantification of NH₂OH by colorimetric methods were not successful, suggesting the rapid transformation of *NH₂OH intermediate, which must be readily captured by ketones and utilized for C-N coupling. The whole process was nicely explained by DFT calculations (Figures 4a, S44, and S45). As shown in Figure 4a, the desorption of *NH₂OH from the catalyst was an endothermic process, thus disfavoring the formation of free NH₂OH. On the other hand, the reduction of *NH₂OH intermediate to both NH₃ and cyclohexanone oxime was exothermic. The reduction of *NH₂OH to NH₃ was moderately exothermic by 1.3 kcal mol⁻¹, but in the presence of cyclohexanone, the oxime formation by C-N coupling was largely exothermic by 13.2 kcal mol⁻¹. It was clear that the product selectivity was

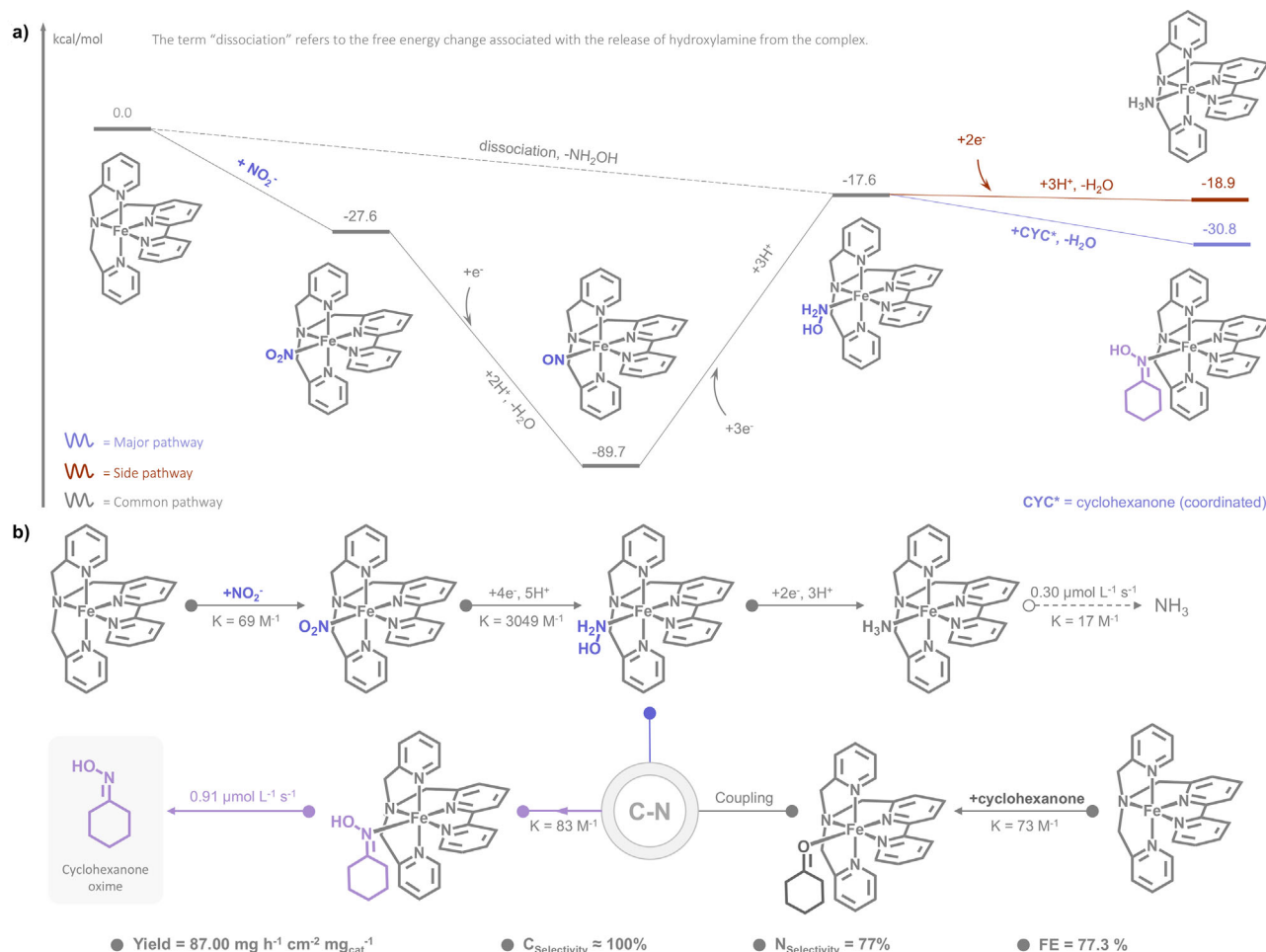


Figure 4. a) Gibbs energy diagram (in kcal mol⁻¹) for NO₂⁻ reduction pathway over FeBPAbipyH/CNT@CP electrode. b) Proposed mechanism for cyclohexanone oxime and ammonia electrosynthesis by FeBPAbipyH. K represents the binding constant between the catalyst and the active species.

determined by the different energies of FeBPAbipyH after coordination with NH₃ and cyclohexanone oxime, *NH₂OH preferably reacted with ketone rather than further reduction to NH₃. The reduction of *NO to *NH₂OH was the most endothermic and thus the rate-limiting step. The coordination of FeBPAbipyH with cyclohexanone was exothermic by 11.0 kcal mol⁻¹, which corroborated the favorable coordination with cyclohexanone (Figure S45). All of the results show that cyclohexanone oxime is formed by condensation of *NH₂OH and *CYC on the electrode, not in electrolyte solution.

In light of the above experimental results, the reaction mechanism for cyclohexanone oxime synthesis catalyzed by FeBPAbipyH was proposed (Figure 4b). FeBPAbipyH interacted with both cyclohexanone and NO₂⁻ in balance, which kept cyclohexanone intact and reduced NO₂⁻ modestly to NH₂OH. Here, a small portion of hydroxylamine proceeded further N–H bond formation to afford ammonia, but the majority of hydroxylamine was captured by cyclohexanone to generate cyclohexanone oxime: the formation rate of cyclohexanone oxime was measured to be 0.91 μmol L⁻¹ s⁻¹, while ammonia synthesis proceeded at a much slower rate of 0.30 μmol L⁻¹ s⁻¹. The refrained N–H bond formation,

more exothermic NO₂⁻-to-oxime than NO₂⁻-to-NH₃ pathway, along with concurrent and adjacent binding with NH₂OH and cyclohexanone of the FeBPAbipyH catalyst, contributed to N–C bond formation three times faster than N–H and O–H bond formation. The matched concentration ratio of C- and N-sources close to 1:1 maximized adjacent C–N coupling to yield cyclohexanone oxime and regenerate catalyst. Fresh cyclohexanone and NO₂⁻ substrates then quickly adsorb on the regenerated catalyst at a ratio close to 1:1 again, thus ensuring the continuous generation of cyclohexanone oxime.

Synthesis of Cyclohexanone Oxime Directly from Air

The successful cyclohexanone oxime synthesis using cyclohexanone and NO₂⁻ encouraged us to use ambient air (78% N₂ + 21% O₂) as a free and abundant N-source to furnish step-economic and sustainable air-to-cyclohexanone oxime conversion in two steps. First, 1 atm. of air was passed through a spark discharger, where N₂ and O₂ were activated by plasma to produce NO_x, followed by NaOH treatment to obtain predominantly NaNO₂. The spark discharger was a commercial neon-lamp power supply working with household

220 V 50 Hz electricity, which continuously delivered NO_2^- at a steady rate of $779 \mu\text{mol h}^{-1}$ and promised energy efficiency of $5.10 \text{ kWh mol}^{-1}$ (Figure S46). Using as-obtained NaNO_2 instead of the reagent-grade one, the yield and FE of cyclohexanone oxime were $61.73 \text{ mg h}^{-1} \text{ cm}^{-2} \text{ mg}_{\text{cat}}^{-1}$ and 64.49% after 2 h electrolysis on the FeBPAbipyH/MWCNTs@CP electrode (Figure S47). After continuous electrolysis for 6 h, the yield and FE of cyclohexanone oxime remained unchanged, showing excellent reproducibility and stability of the FeBPAbipyH/MWCNTs@CP electrode. It was pertinent to mention that the obtained cyclohexanone oxime and NH_3 could be directly separated by extraction, where the organic phase delivered pure cyclohexanone oxime solid and distillation of the aqueous phase afforded inorganic NH_4Cl salt (Figure S48). The techno-economic analysis (TEA) considering the whole plasma-driven N_2 oxidation, electrocatalytic NO_x^- reduction and product separation processes using the best catalysts and optimum operating conditions indicated that cyclohexanone oxime could be synthesized at a promising cost of $\$2709 \text{ ton}^{-1}$ with an electricity price of $\$0.03 \text{ per kWh}$, which is much lower than the breakeven point ($\sim \$10\,000 \text{ ton}^{-1}$) (Supplementary Note 2). The preparative synthesis of high-purity cyclohexanone oxime fully demonstrates the potential for sustainable and step-economic synthesis of cyclohexanone oxime by tandem plasma N_2 activation and electrocatalytic NO_x^- reduction from ambient air in aqueous solution and with sustainable electricity.

Conclusion

In summary, well-defined molecular iron polypyridine catalysts anchored on MWCNTs are used to accomplish innovative synthesis of cyclohexanone oxime from ambient air by integrating plasma air oxidation and electrochemical C–N coupling. Experimental results show that the FeBPAbipyH catalyst loaded on CNT favors the coordination of cyclohexanone, which is beneficial to the coupling of cyclohexanone with nitrogenous intermediates. At the same time, FeBPAbipyH has a strong interaction with $^*\text{NH}_2\text{OH}$ to stabilize the active NH_2OH intermediate. The commensurable coordination constants with NO_2^- and cyclohexanone substrates favor rapid and intimate C–N coupling, in which cyclohexanone oxime was more exothermic by $11.9 \text{ kcal mol}^{-1}$ and more rapid by a factor of 3 than NH_2OH over-reduction to form NH_3 . Therefore, the FeBPAbipyH/MWCNTs@CP cathode, at the potential of -0.40 V vs. RHE, realized an exceptional mass-specific cyclohexanone oxime production rate of $87.00 \text{ mg h}^{-1} \text{ cm}^{-2} \text{ mg}_{\text{cat}}^{-1}$, 77.3% Faradic efficiency, exclusive C–N coupling over cyclohexanone hydrogenation, and good stability. In situ FTIR, in situ Raman spectra, and DFT calculation confirmed the formation of absorbed hydroxylamine and C=N bonds. In tandem N_2 -to-cyclohexanone oxime synthesis, the yield rate of cyclohexanone oxime reached $61.73 \text{ mg h}^{-1} \text{ cm}^{-2} \text{ mg}_{\text{cat}}^{-1}$, and the whole synthetic and separation process is projected to be profitable with a promising cost of $\$2709 \text{ ton}^{-1}$, which is much lower than the breakeven point ($\sim \$10\,000 \text{ ton}^{-1}$). This study, through multielectron and proton transformation of nitrogenous small

molecules, represents a new pathway for the benign, economical, and sustainable production of cyclohexanone oxime as an alternative to the current existing processes.

Acknowledgements

The authors are grateful for financial support from the National Key Research and Development Program of China (2022YFA0911900, 2022YFA1502900, and 2021YFA1500800), the National Natural Science Foundation of China (22088102 and 22193013), the Strategic Priority Research Program of the Chinese Academy of Science (XDB0960100), and New Cornerstone Science Foundation.

Conflict of Interests

The authors declare no conflict of interest.

Data Availability Statement

The data that support the findings of this study are available from the corresponding author upon reasonable request.

Keywords: C–N coupling • Cyclohexanone oxime • Electrocatalysis • Iron polypyridine complex • Nitrogen fixation

- [1] R. J. Lewis, K. Ueura, X. Liu, Y. Fukuta, T. E. Davies, D. J. Morgan, L. Chen, J. Qi, J. Singleton, J. K. Edwards, S. J. Freakley, C. J. Kiely, Y. Yamamoto, G. J. Hutchings, *Science* **2022**, 376, 615–620.
- [2] J. M. Thomas, R. Raja, *Proc. Natl. Acad. Sci. USA* **2005**, 102, 13732–13736.
- [3] B. Zong, B. Sun, S. Cheng, X. Mu, K. Yang, J. Zhao, X. Zhang, W. Wu, *Engineering* **2017**, 3, 379–384.
- [4] J. Xian, S. Li, H. Su, P. Liao, S. Wang, Y. Zhang, W. Yang, J. Yang, Y. Sun, Y. Jia, Q. Liu, Q. Liu, G. Li, *Angew. Chem. Int. Ed.* **2023**, 62, e202304007.
- [5] J. Xian, S. Li, H. Su, P. Liao, S. Wang, R. Xiang, Y. Zhang, Q. Liu, G. Li, *Angew. Chem. Int. Ed.* **2023**, 62, e202306726.
- [6] P. Liao, J. Kang, R. Xiang, S. Wang, G. Li, *Angew. Chem. Int. Ed.* **2023**, 63, e202311752.
- [7] Y. Wu, W. Chen, Y. Jiang, Y. Xu, B. Zhou, L. Xu, C. Xie, M. Yang, M. Qiu, D. Wang, Q. Liu, Q. Liu, S. Wang, Y. Zou, *Angew. Chem. Int. Ed.* **2023**, 62, e202305491.
- [8] Y. Sheng, J. Xie, R. Yang, H. Yu, K. Deng, J. Wang, H. Wang, L. Wang, Y. Xu, *Angew. Chem. Int. Ed.* **2024**, 63, e202410442.
- [9] J. Sharp, A. Ciotti, H. Andrews, S. R. Udayasurian, M. García-Melchor, T. Li, *ACS Catal.* **2024**, 14, 3287–3297.
- [10] L. Luo, L. Li, L. Xu, Y. Yan, S. Zhang, H. Zhou, Z. Li, M. Shao, X. Duan, *CCS Chem* **2025**, 7, 266–278.
- [11] Y. Wu, J. Zhao, C. Wang, T. Li, B. H. Zhao, Z. Song, C. Liu, B. Zhang, *Nat. Commun.* **2023**, 14, 3057.
- [12] X. Zhang, H. Jing, S. Chen, B. Liu, L. Yu, J. Xiao, D. Deng, *Chem. Catal.* **2022**, 2, 1807–1818.
- [13] S.-L. Meng, C. Zhang, C. Ye, J.-H. Li, S. Zhou, L. Zhu, X.-B. Li, C.-H. Tung, L.-Z. Wu, *Energy Environ. Sci.* **2023**, 16, 1590–1596.
- [14] S.-L. Meng, C. Ye, X.-B. Li, C.-H. Tung, L.-Z. Wu, *J. Am. Chem. Soc.* **2022**, 144, 16219–16231.
- [15] S.-L. Meng, X.-B. Li, C.-H. Tung, L.-Z. Wu, *Chem* **2021**, 7, 1431–1450.

- [16] D.-S. Zhang, Y.-P. Liang, Y. Yang, C.-H. Tung, L.-Z. Wu, *Chin. Sci. Bull.* **2025**, *70*, 835–849.
- [17] S. Zhou, L.-J. Zhang, L. Zhu, C.-H. Tung, L.-Z. Wu, *Adv. Mater.* **2023**, *35*, 2300923.
- [18] L. Zhu, Y.-X. Wang, L.-J. Chen, J. Li, S. Zhou, Q.-Q. Yang, X.-Z. Wang, C.-H. Tung, L.-Z. Wu, *Angew. Chem. Int. Ed.* **2025**, *64*, e202418156.
- [19] H.-X. Wang, H.-Z. Liu, Y.-Q. Zhang, S.-L. Meng, X.-Z. Wang, C. Ye, X.-B. Li, R.-Z. Liao, C.-H. Tung, L.-Z. Wu, *CCS Chem* **2024**, *6*, 2971–2981.
- [20] Y. Pan, Y. Zou, C. Ma, T. T. T. Nga, Q. An, R. Miao, Z. Xia, Y. Fan, C.-L. Dong, Q. Liu, S. Wang, *J. Am. Chem. Soc.* **2024**, *146*, 19572–19579.
- [21] S. Zhou, L.-J. Zhang, J. Li, C.-H. Tung, L.-Z. Wu, *Angew. Chem. Int. Ed.* **2024**, *63*, e202407836.
- [22] F. Liu, X. Gao, R. Shi, Z. Guo, E. C. M. Tse, Y. Chen, *Angew. Chem. Int. Ed.* **2023**, *135*, e202300094.
- [23] X. Wu, Z.-J. Zhao, X. Shi, L. Kang, P. Das, S. Wang, S. Chu, H. Wang, K. Davey, B. Zhang, S.-Z. Qiao, J. Gong, Z.-S. Wu, *Energy Environ. Sci.* **2024**, *17*, 3042–3051.
- [24] Z. Zhu, Y. Jiang, L. Xu, Q. An, T. T. T. Nga, J. Chen, Y. Fan, Q. Liu, C.-L. Dong, S. Wang, Y. Zou, *Adv. Mater.* **2025**, *37*, 2409864.
- [25] J. Shao, Y.-F. Zhang, S.-Z. Xue, Z.-Y. Li, X. Li, B. Liang, T.-Z. Li, H. Dong, Y.-W. Zhang, *Inorg. Chem. Front.* **2024**, *11*, 5286–5298.
- [26] F. Liu, X. Gao, Z. Guo, E. C. M. Tse, Y. Chen, *J. Am. Chem. Soc.* **2024**, *146*, 15275–15285.
- [27] S. Jia, X. Tan, L. Wu, X. Ma, L. Zhang, J. Feng, L. Xu, X. Song, Q. Zhu, X. Kang, X. Sun, B. Han, *Chem. Sci.* **2023**, *14*, 13198–13204.
- [28] B. N. Brown, K. J. Robinson, Q. C. Durfee, D. Kekilli, M. A. Hough, C. R. Andrew, *Inorg. Chem.* **2020**, *59*, 14162–14170.

Manuscript received: March 21, 2025

Revised manuscript received: April 16, 2025

Accepted manuscript online: April 18, 2025

Version of record online: ■■■■■

Research Article

Electrocatalysis

C. Zhang, S.-L. Meng, Y.-N. Jing, C. Wang,
X.-L. Zhang, H.-X. Wang, C.-H. Tung,
L.-Z. Wu* ————— **e202506546**

Synergistic C—N Coupling for Efficient
Cyclohexanone Oxime Synthesis from
Ambient Air by Supported Molecular
Catalysts

A molecular catalyst is demonstrated to be unique for oxime synthesis under mild conditions. The mass-specific efficiency of $87.00 \text{ mg h}^{-1} \text{ mg}_{\text{cat}}^{-1}$, Faradaic efficiency (FE) of 77.3%, and exclusive carbon selectivity are the best known to date in H-cell. The whole synthetic and separation process is projected to be profitable with a promising cost of $\$2709 \text{ ton}^{-1}$, which is much lower than the breakeven point ($\sim \$10\,000 \text{ ton}^{-1}$). Mechanistic studies reveal the intimate interaction with both cyclohexanone and NO_2^- , and selective NO_2^- -to- NH_2OH catalytic reduction for C—N bond in situ. The unprecedented results obtained offer an ideal platform for the benign, economical, and sustainable production of cyclohexanone oxime as an alternative to the current existing processes.

